Thermo-Hydraulic Analysis of Slightly Inclined Finned Channel under Natural Convection

K. Roy[1†], B. Das[2], K. K. Pathak[3] and A. Giri[4]

[1]*Department of Mechanical Engineering, Regional Institute of Science and Technology, Baridua, Ri-Bhoi, Meghalaya, 793101, India*
[2]*Department of Mechanical Engineering, National Institute of Technology, Silchar, Assam, 788010, India*
[3]*Department of Mechanical Engineering, Girijananda Chowdhury Institute of Management and Technology, Guwahati, Assam, 781017, India*
[4]*Department of Mechanical Engineering, North Eastern Regional Institute of Science and Technology, Nirjuli-791109, India*

†*Corresponding Author Email: krishna_rs@mech.nits.ac.in*

ABSTRACT

The influence of slight inclination, 'α' (i.e., 10°, 15°, and 20°) of the channel comprised of shrouded vertical rectangular non-isothermal fin array has been computationally investigated. Simulations are performed to obtain the convective coefficient of heat transfer for the different dimensionless fin spacing ($S^* = 0.2, 0.3, 0.5$), non-dimensional fin tip to shroud clearances ($C^* = 0.1, 0.2$ and 0.3), Grashof numbers (Gr= 1.08×10^5, 4.42×10^5 and 11.5×10^5), fin lengths (L= 0.25m and 0.5m) and fin heights (H= 0.025m, 0.04m, and 0.055m). Hydrodynamic behavior of the fluid indicates that a significant amount of flow reversal occurs near the entrance of the channel at very low inclination which vanishes with the increase in inclination. Further, at higher length, reverse flow is found to occur only in the clearance zone. An increase in the value of 'α' from 10° to 20°, results in enhancement of convective coefficient up to a maximum of 161%. An increase in the value of fin spacing from 0.2 to 0.5 results in the enhancement of the convective heat transfer coefficient. At α= 15° and 20°, the heat transfer is enhanced by 84.1% and 101.6%, respectively, while at α=10°, the same is reduced by 33.3%. At lower fin spacing ($S^* < 0.3$) increase in C^* tends to reduce the efficiency. Further, the efficiency of the finite conductive fin is found to reduce by almost 8% with an increase in Grashof number.

Keywords: Grashof number; Inclination; Clearance; Convective coefficient; Fin efficiency.

NOMENCLATURE

C	clearance	Pr	Prandtl number
C^*	dimensionless clearance	Q	overall heat transfer
Gr	Grashof number	S	inter-fin spacing
H	height of fin	S^*	dimensionless spacing
h	convective heat transfer coefficient	T	temperature
k	thermal conductivity	t	thickness of fin
L	length of the fin	u,v,w	velocity components in x-, y- and z-directions
L^*	non-dimensional length of the fin		
Nu	overall Nusselt number	U,V,W	non-dimensional velocity components in $x,y,$ and z directions, uH/υ, vH/υ, and wH/υ
p	total pressure defect, p_o-p_s		
p'	cross-stream pressure		
$\bar{p}$	average pressure defect over the cross-section	x,y,z	cross stream and axial coordinates
P^*	dimensionless axial pressure defect	X,Y,Z	non-dimensional cross-stream and axial coordinates, x/H, y/H, and z/H

Greek symbols
α	inclination angle		
β	thermal volumetric expansion coefficient	Subscripts	
γ	thermal diffusivity	f	fin
Ω	fin conductance parameter	l	local

ΔT	temperature difference	*in*	inlet
ρ	density	*m*	mean
μ	dynamic Viscosity	o	ambient
υ	momentum diffusivity	*w*	wall
θ	dimensionless temperature		

1. INTRODUCTION

A rapid removal of heat from thermal devices or components is the most important requirement for better performance of the devices and to upsurge its lifespan. At the same time, it reduces the maintenance necessities to a lower level. Thus, better thermal management of these devices is important as well as essential. Heat sinks are attached widely to various engineering components (for example transformers, boilers, car radiators, and solar air collectors, etc.) for removing the heat quickly. The design and orientation of these heat sinks always play a significant role in enhancing heat transport under different modes. The phenomenon of natural convection heat transfer is always present in any thermal devices. Thus, proper and careful examination is needed to perform natural convective analysis over any physical configurations.

For a vertical rectangular fin array, the study of natural convection is performed by Welling and Wooldridge (1965) and specifically mentioned an optimum fin height with spacing for a maximum heat transfer. Harahap and McManus (1967) experimentally investigated for similar fin array but in a horizontal orientation. Leung *et al.* (1985) followed these studies and focused the investigation of the optimum inter-fin spacing on a vertical rectangular fin array. In another investigation, Karki and Patankar (1987) reported the presence of variation of the flow characteristics with clearance from the fin tip to the shroud. An additional chimney has been integrated with the exit of the fin array and results of enhancement in the heat transfer are presented experimentally by Fisher and Torrance (1999). Dialameh *et al.* (2008) presented the impact of a shorter length of fin for free convection from a horizontal fin array. Researchers have also investigated the modification of the fin physical geometry. Experimental comparison between the plated and pin fin is conducted by Micheli *et al.* (2016) at micro-scale. Also, to reduce the fin material and improve the natural convective heat transfer the variation of fin height is investigated by Jeon and Byon (2017), Pathak *et al.* (2018), and Huang *et al.* (2019). Davoodi and Yaghoubi (2018) experimentally compared triangular zig-zag fins with rectangular plated fins for maximum free convection. Feng *et al.* (2018) analyzed both numerically and experimentally the modification from the convectional plated fin array to the cross-fin array for a horizontal arrangement. Mousavi *et al.* (2018) numerically investigated the heat transfer for interrupted, staggered, and capped fins. Dindarloo and Payan (2019) studied the effect of fin thickness and length on heat transfer. Shi *et al.* (2019) developed an optimized geometry for a micro-channel heat sink. Rippling fin shaped heat sink at a

vertical position is investigated by Ghandouri *et al.* (2020) for natural convection and obtained results for reduced weight to surface ratio, which enhances the performance. Roy and Das (2021) investigated the effect of variable properties, such as thermal conductivity, density, viscosity of the working medium in the free convection heat transfer from a finned channel.

For mixed convection heat transfer, Al-Sarkhi *et al.* (2003), Giri and Das (2012), and Das and Giri (2014) studied numerically all the parametric variation effects such as clearance, spacing, height for a vertical fin array. Zhang *et al.* (2015) numerically analyzed the variation of the ratio between the wavelength to the fin length and studied the effect of different attack angles for the serrated fins. Also, Ahmed *et al.* (2016) numerically studied the ribbed flat plated fins and presented the optimized design for better thermal performance. Chen *et al.* (2017) studied numerically and experimentally the heat transfer and fluid flow characteristics of a plate-fin heat sink. Again, Roy and Das (2020) investigated mixed convection from an isothermal and non-isothermal plated inclined fin array, respectively.

Attention may now be turned on to the effect of inclination on the convective heat transfer. Pertinent literature shows both natural as well as mixed convection the significance of the inclination angle of the fin-base system. In 1963, an experimental investigation on natural convection at three different inclination positions (i.e., 0°, 45°, and 90°) is reported by Starner and McManus (1963). Again Mittelman *et al.* (2007) reported the effect of inclination from a downward-facing fin array. Tari and Mehrtash (2013) and Mehrtash and Tari (2013) developed a correction along with a detailed analysis of heat transfer has been performed. Shen *et al.* (2014) concerned about the LED applications of four rectangular fin heat sinks in 8 different orientations and analyzed its performances. In an inclined rectangular channel, the effect of local flow modulation using circular rotating cylinders on heat transfer is computationally investigated by Hasan *et al.* (2017). Meng *et al.* (2018) performed computational analysis for different mount angles and obtained the best heat transfer performance at an angle of 90°. Also, Yang and Yeh (2019) studied the mixed convection heat transfer in a channel with staggered fins numerically. Another interesting experimental investigation by Homod *et al.* (2019) presented the effect of longitudinal and lateral inclination angle on mixed convection. Karlapalem *et al.* (2019) analyzed the orientation effect for free convection on a branched fin.

The survey of the literature describes the use of an inclined-based fin array under a different mode of heat transfer. For a close-packed model, slight

inclinations of the base might provide useful results. Moreover, the effect of slight inclination of the base from the horizontal position is highly needed as delineated by the article of Boutina and Bessaïh (2011) for a series of protrusions assumed to be electronic components kept in an angled channel. Tari and Mehrtash (2013a) reported for both slight inclination and horizontal orientation and developed a correlation for the same. Also, Roy *et al.* (2019) performed natural convection investigation from an inclined channel at a higher inclination. Thus, the scope to unveil the thermo-hydraulic behavior in the low inclined channel remains open. In this essence, the study of the shrouded slightly inclined-based fin heat sinks undergoing natural convection might give a better understanding of the problem. Besides, the parametric study of this configuration will be beneficial for heat sink designers. Moreover, the report of Alta *et al.* (2010) strongly supports the importance of the slight inclination of the base plate in a solar air heater problem. Thus, an attempt has been made in the present work to investigate the hydrodynamic and thermodynamic analysis of a shrouded slightly inclined-based (i.e., 10°, 15°, and 20°) fin heat sinks undergoing natural convection.

2. PHYSICAL DESCRIPTION AND MATHEMATICAL FORMULATION

2.1 Physical Configuration

Figure 1a depicts the array of fins attached to an angled hot base plate which maintains an angle (α) of 10°, 15°, and 20° to the horizontal. The fin height, length, and thickness of the fins are designated by 'H', 'L', and 't', respectively as shown in Fig. 1a. The spacing between the two fins is denoted by 'S'. An adiabatic shroud is placed in front of the fin array maintaining a clearance of 'C' to encourage the buoyancy effect. In Fig. 1b, the cross-section of the duct required for the present analysis is presented. As all the ducts formed by the fins are identical, only one of such ducts is needed to be analyzed. Thus, a uniform rectangular duct of dimension L×(H+C)×(S) is formed by an adiabatic shroud, fin, and base. The gravity force acts vertically downward. Along the base, fin height and length, *x*-, *y*-, *z*-axes are considered respectively. There is no heat generation within the fin array of any kind. The ambient is considered as T_o and a higher temperature (T_w) is maintained at the base. An upward natural convective flow is induced due to the buoyancy differences arising from the prescribed temperature differences. The following section describes the governing equations required to formulate the present investigation.

2.2 Governing Equations

The governing equations of continuity, momentum, and energy required to describe the physical configuration are written in a representative form which is given in the Eqn. (1-6). Air is considered as the working fluid. And steady, laminar and incompressible flow is assumed. Further, convection dominates the flow in the axial direction, and diffusion is treated negligible (Das and Giri (2014)
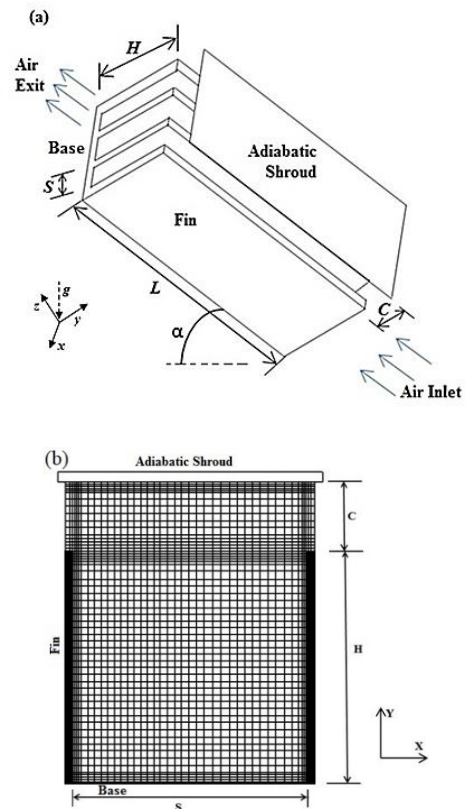
and Roy *et al.* (2019)).

Fig. 1(a) Schematic diagram of the inclined shrouded fin array and (b) cross-section of the duct section.

Continuity equation

$$\frac{\partial u}{\partial x} + \frac{\partial v}{\partial y} + \frac{\partial w}{\partial z} = 0 \qquad (1)$$

x-momentum equation

$$\left(u\frac{\partial u}{\partial x} + v\frac{\partial u}{\partial y} + w\frac{\partial u}{\partial z}\right) = -\frac{1}{\rho}\frac{\partial p}{\partial x} + \frac{\mu}{\rho}\left(\frac{\partial^2 u}{\partial x^2} + \frac{\partial^2 u}{\partial y^2} + \frac{\partial^2 u}{\partial z^2}\right) \quad (2)$$

y-momentum equation

$$\left(u\frac{\partial v}{\partial x} + v\frac{\partial v}{\partial y} + w\frac{\partial v}{\partial z}\right) = -\frac{1}{\rho}\frac{\partial \acute{p}}{\partial y} + \frac{\mu}{\rho}\left(\frac{\partial^2 v}{\partial x^2} + \frac{\partial^2 v}{\partial y^2} + \frac{\partial^2 v}{\partial z^2}\right) +$$
$$g\beta cos\alpha(T - T_0) \qquad (3)$$

z-momentum equation

$$\left(u\frac{\partial w}{\partial x} + v\frac{\partial w}{\partial y} + w\frac{\partial w}{\partial z}\right) = -\frac{1}{\rho}\frac{\partial \acute{p}}{\partial z} + \frac{\mu}{\rho}\left(\frac{\partial^2 w}{\partial x^2} + \frac{\partial^2 w}{\partial y^2} + \frac{\partial^2 w}{\partial z^2}\right) +$$
$$g\beta sin\alpha(T - T_0) \qquad (4)$$

Energy equation

$$\rho\left(u\frac{\partial T}{\partial x} + v\frac{\partial T}{\partial y} + w\frac{\partial T}{\partial z}\right) = \frac{k}{C_p}\left(\frac{\partial^2 T}{\partial x^2} + \frac{\partial^2 T}{\partial y^2} + \frac{\partial^2 T}{\partial z^2}\right) \qquad (5)$$

Fin conduction equation,

$$\left(\frac{\partial^2 T}{\partial x^2} + \frac{\partial^2 T}{\partial y^2}\right) = 0 \qquad (6)$$

2.3 Initial and Boundary Conditions

For the current investigation, in the axial direction, the convection dominates over diffusion and hence later can be treated as negligible. Therefore, the inlet conditions along with the boundary conditions are

needed to be defined before proceeding towards the solution. However, the identification of the unknown inlet streamwise velocity is required as the problem is buoyancy-driven. The pressure defect is assumed to be zero at the entry and the exit. Again, with the above-mentioned approximation, with several guessed entry velocities iterations are performed. Further, the correct entry velocity is recognized for the arrangement having no pressure defects at the outlet (Pathak *et al.* (2018), and Roy *et al.* (2019)). The inlet temperature is considered to be the ambient temperature. Further, at the vicinity of the solid surfaces "no-slip" and impermeability conditions are deployed. The shroud surface is considered to be solid, impermeable, and adiabatic. At the plane in the clearance over the fin tip, zero normal velocity and normal gradients of the other velocities and temperature are considered. Furthermore, the fin and base are at an identical temperature and an insulated fin tip is assumed. Mathematical forms of the boundary conditions are defined in Table 1.

Table 1: Boundary conditions of the present problem

At the base $0 \leq x \leq S$, $y = 0$, $0 \leq z \leq L$	$u = v = w = 0$, $T = T_w$
At the plane in the clearance above the fin tip $x = 0$, $H \leq y \leq H+C$, $0 \leq z \leq L$	$u=0$, $\frac{\partial v}{\partial x}=0, \frac{\partial w}{\partial x}=0, \frac{\partial T}{\partial x}=0$
At the shroud $0 \leq x \leq S$, $y=H+C$, $0 \leq z \leq L$	$u = 0$, $v = 0$, $w = 0$, $\frac{\partial T}{\partial x}=0$
On the fin surface $x = 0$, $0 \leq y \leq H$, $0 \leq z \leq L$	$u= v = w = 0$, $T = T_f$
Fin boundary conditions at the base and tip $x=0$, $0 \leq z \leq L$	At $y = 0$, $T = T_w$, and at $y = H$, $\frac{\partial T}{\partial y}=0$

2.4 Overall Convective Coefficient and Nusselt Number

The design and construction of thermoelectric devices always require the range of magnitude of overall heat transfer. Also, it is arduous to evaluate the actual heat transfer rate due to the varying bulk temperature. The temperature difference (i.e., between the base and ambient) a mathematical formulation of the fin-base arrangement is applied to evaluate the total heat transfer (Q), average heat flux (*q*), overall convective coefficient (*h*), and overall Nusselt number (Nu) are as follows,

$$Q = Q_{fin} + Q_{base}$$

$$= \left(\int_0^L \int_0^H k_f \frac{\partial T}{\partial x}\Big|_{x=0} dydz\right) + \left(\int_0^L \int_0^S k_f \frac{\partial T}{\partial x}\Big|_{y=0} dxdz\right) \quad (7)$$

$$q = \frac{Q}{(H+S)L}, \quad h=q/(T_w-T_o) \quad (8)$$

$$Nu = \frac{\int_0^L \left[\int_0^H \frac{\partial T}{\partial x}\Big|_{x=0} dy - \int_0^S \frac{\partial T}{\partial y}\Big|_{y=0} dx\right]dz}{(H+S)L(T_w-T_o)} \quad (9)$$

The governing equations, inlet, and boundary conditions along with the equations are required to evaluate heat transfer coefficient and to complete the mathematical formulation. Furthermore, several parameters govern the current investigation are considered, such as Inclination angle (α), Prandtl number (Pr), Grashof number (Gr), fin conductance parameter (Ω), non-dimensional inter-fin spacing (S*), and non-dimensional clearance (C*). The system of equations is solved in the following sections using computational procedures.

3. COMPUTATIONAL METHOD

The present problem is solved with the application of the SIMPLER algorithm elucidated in Patankar (1980). To determine the pressure field, it is essential to satisfy the continuity equation. The discretization on a staggered mesh is performed by the power-law scheme for the combined diffusive and convective terms of cross-stream coordinates. And the convective terms are evaluated along the stream-wise coordinates applying the backward-difference method. Moreover, a sufficient number of outer iterations is performed as an iterative implicit method at each axial section. The developments of staggered grids are in rectangular shapes in all three directions (i.e., *x*-, *y*- and *z*- direction). The convergence is obtained when the desired accuracy is achieved between the consecutive iterations. Also, Tri-Diagonal Matrix Algorithm (TDMA) is applied to evaluate equations sequentially. Further, adequate under-relaxation factors are applied to reduce computational errors in the results. Again, close to the entry in the stream-wise z-direction non-uniform grids are developed to evaluate the development of the boundary layer. The present computational code is appropriately modified from previously developed code formulated by Giri and Das (2012), Das and Giri (2014), and Roy *et al.* (2019). The grid sensitivity test and the validation with previously performed experimentation on an inclined fin array are discussed in the next subsection.

3.1 Grid Independence test

A grid sensitivity test is performed for L^*=20, Gr= 1.08×10^5, C^*= 0.10, S^*=0.2, S^*= 0.3 and S^*= 0.5 and at α= 10°. The grid sizes are varied particularly for *x*- and *y*- direction, since the fin spacing and height are in *x*- and *y*- direction, respectively. The variation in the Overall Nusselt number (Nu) value is tabulated in Table 2 for various grid combinations and found to be rational within1.2%.

3.2 Validation

The validation of the numerical solution is performed with the experimental results of Starner and McManus (1963) with four sets of different fin arrangements. The experiment (Starner and McManus (1963)) is performed at α= 45° with three

Table 2: Grid independence test for L^*= 20, Gr= 1.08×10^5, C^*= 0.10

Fin Spacing (S^*)	Inclination angle (α)	Grid Size ($X \times Y \times Z$)	Overall Nusselt Number (Nu)
0.2	10°	16 × 30 ×100	0.3399
		18 × 32 ×100	**0.3440**
		20 × 34 ×100	0.3474
0.3	10°	18 × 30 ×100	0.3149
		20 × 32 ×100	**0.3188**
		22 × 34 ×100	0.3215
0.5	10°	22 × 34 ×100	0.2275
		24 × 36 ×100	**0.2296**
		26 × 38 ×100	0.2308

Table 3: Experimental validation with Starner and McManus (1963)

Fin condition	Difference of surface and ambient temperature (ΔT °C)	Starner and McManus (1963) h (W/m² K)	Present Results h (W/m² K)	% variation
Set 1 (H= 0.0127 m, S= 0.00635m, α= 45°)	15.56	1.5889	1.6711	4.91
	37.78	2.0995	2.1898	4.12
	82.22	2.7237	2.8797	5.41
Set 2 (H= 0.0381 m, S= 0.00635m, α= 45°)	18.33	1.9293	2.0692	6.76
	40.56	2.5535	2.7112	5.81
	82.22	3.2912	3.4188	3.73
Set 3 (H= 0.00635m, S= 0.00635m, α= 45°)	18.33	1.9861	2.0848	4.73
	40.56	2.0428	2.1616	5.49
	82.22	2.8373	3.0156	5.91
Set 4 (H= 0.0254 m, S= 0.00795m, α= 45°)	18.33	2.4400	2.5801	5.43
	40.56	3.1209	3.2702	4.56
	82.22	3.6884	3.8128	3.26

sets of temperature differences (ΔT) which are used as input to the numerical code. The validation is tabulated in Table 3. From the results, it is observed

that the results of the present investigation bear a good agreement with the experimental findings.

4. RESULTS AND DISCUSSION

The crux of the present investigation is to study the effect of slight inclination (i.e., α=10°, 15°, and 20°) of the base plate on heat and fluid flow over a rectangular shrouded fin array. All the governing parameters are tabulated in Table 4. Also, at an average value of ambient and base temperature, the properties of fluid such as thermal conductivity, viscosity, and density are evaluated. The working fluid for the present investigation is chosen as air and its properties are calculated following the Das and Giri (2014) and Roy *et al.* (2019). Those are listed as follows:

Thermal Conductivity of Air:

$$k = \frac{T^{(\frac{3}{2})} \times 1.195 \times \frac{1}{10^3}}{118+T} \tag{10}$$

Viscosity of Air:

$$\mu = \frac{T^{(\frac{3}{2})} \times 1.488 \times \frac{1}{10^6}}{118+T} \tag{11}$$

Density of Air:

$$\rho = \frac{21.96 \times 28.93}{\frac{9}{5} \times (T-273.26)+491.69} \tag{12}$$

where, T is the temperature on the Kelvin scale. And the results are described in the subsequent sections.

Table 4: Governing parameters

| Parameters	Range
H (m)	0.025, 0.04, 0.055
L (m)	0.25, 0.5
T_w (ºC)	100
T_o (ºC)	20
t (m)	0.001
k_f (W/m-K)	75
C^*	0.1, 0.2, 0.3
S^*	0.2, 0.3, 0.5
a	10°,15°,20°
Gr	1.08×10^5, 4.42×10^5, 11.5×10^5
Pr	0.71

4.1 W-Velocity Profile

In Fig. 2, the variation of the *W*-velocity profile is illustrated for Gr=1.08×10^5, S^*= 0.20, and C^*=0.10. It is interesting to note that the fluid flow is reversed at certain parametric conditions. At a lower length of the channel (L^*= 10), flow reversal is observed at near the inlet (i.e., Z= 0.75), mid (i.e., Z=5.0) and the outlet (i.e., Z= 9.50) as shown in Fig.2a-c. Further, a close look into the results indicates that as we move towards the downstream (Fig. 2a) location of the flow reversal move from the clearance region towards the base and its magnitude decreases continuously (Fig. 2c). This may be due to the dominance of the blocking effect over the stack effect or chimney effect. However, at the higher

length of the channel, such observations have not been observed. At the mid (i.e., Z=5.0), Fig.2b a genuine profile of the flow phenomenon is obtained. It may also be noted that the deviation of the present trend from the results of Roy *et al*. (2019) may be due to the consideration of higher inclination (>30º) of the channel. As such, the effect of such hydrodynamic behavior on the heat transfer from the inclined channel having the low inclination and lower length would be the point of interest, which has not been paid attention to in the previous studies (Roy *et al*. (2019), Dialameh *et al*. (2008), Das and Giri (2014), Starner and McManus (1963), Tari and Mehrtash (2013) and Shen *et al*. (2014)).

Keeping all other parameters same at α=10°, the length of the channel is increased (i.e., $L^* = 20$) and plotted in Fig.2d-f. It can be observed that near the inlet (i.e., $Z = 1.2$), the similar trend of flow is

observed but its magnitude reduces compare to the case of lower fin length. However, the reverse flow has not been observed near the outlet. This may be due to the chimney effect, which increases with the increase in length of the channel. Figure 2g-l indicates that at a higher inclination angle (α=15° and 20°) with the higher length of the channel, flow reversal has not been occurred at the outlet, due to a higher chimney effect.

Moreover, comparing all the figures, it can be seen that with the increase in the value of the inclination, the magnitude of the maximum value of the *W*-velocity is increased gradually, but the magnitude of reverse flow reduces. A further increase in inclination is expected to diminish the reverse flow both at the inlet and the outlet as shown by Starner and McManus (1963), Das and Giri (2014), and Roy *et al*. (2019).
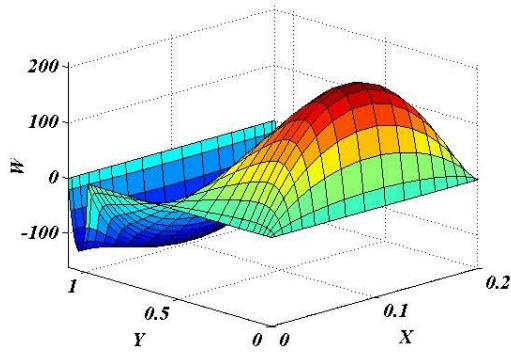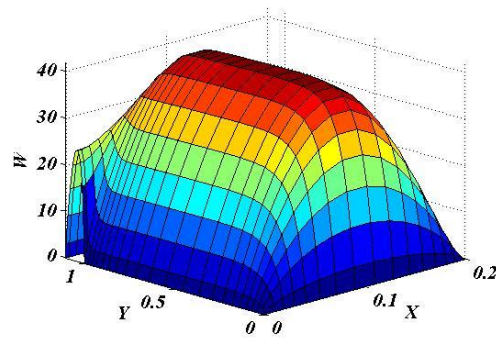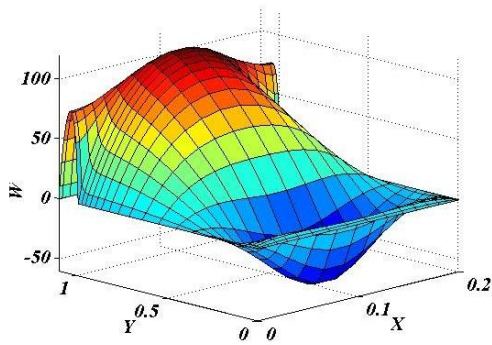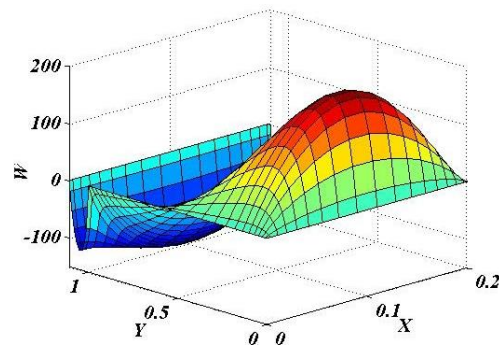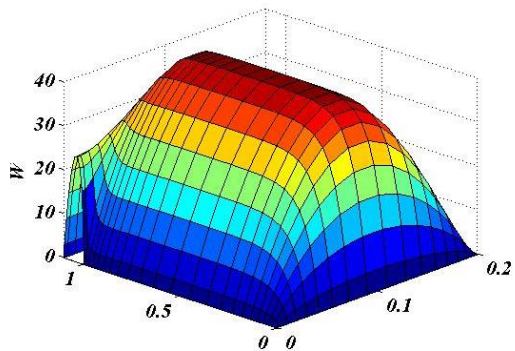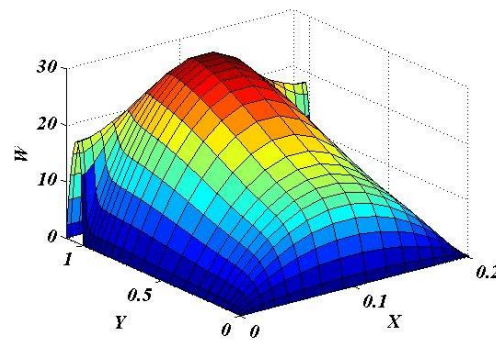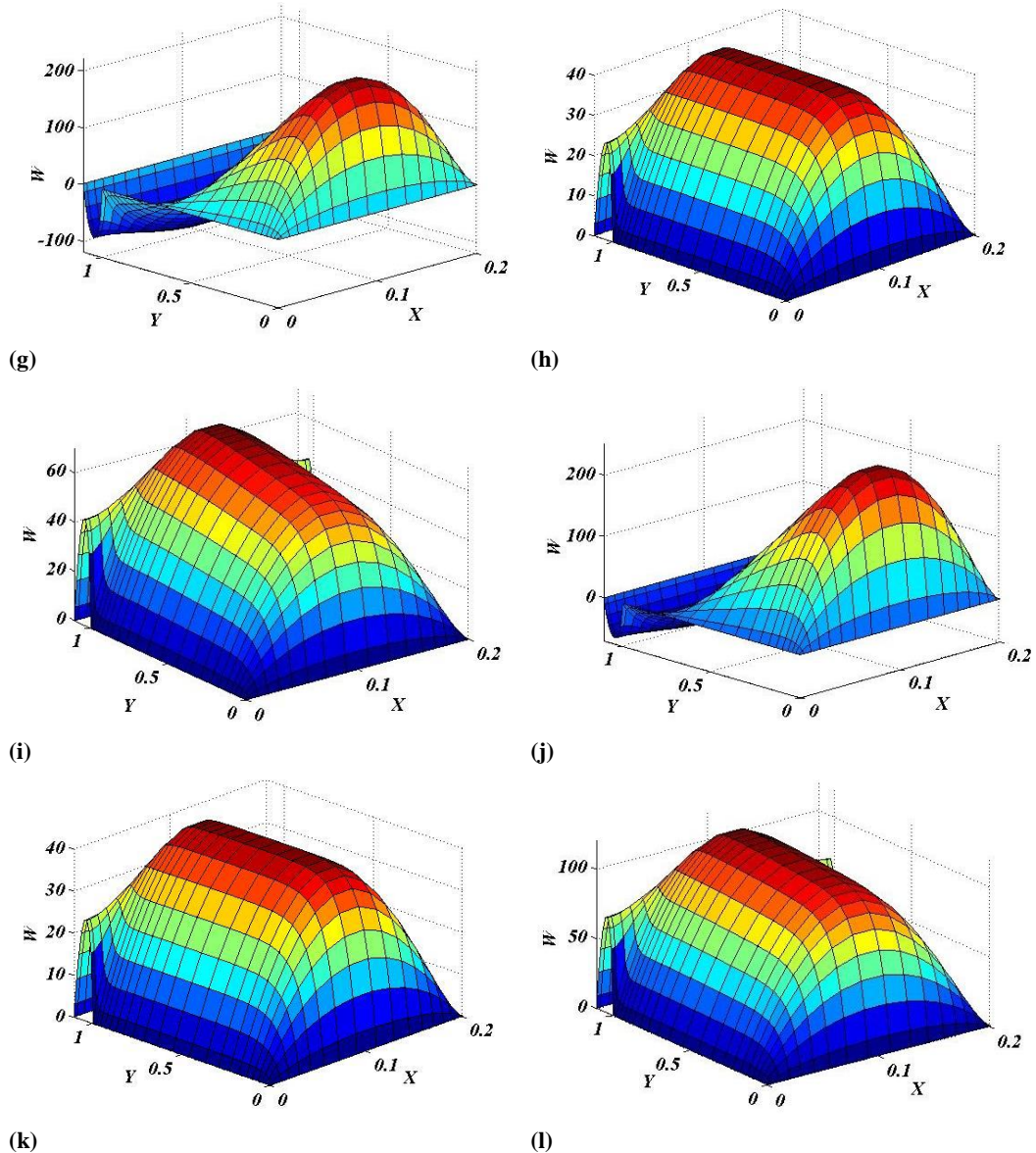

(a) (b) (c) (d) (e) (f)

Fig. 2. W-velocity plot for S^***=0.2,** C^***=0.1, Gr=1.08×10^5 at (a)** L^***=10,** $α$**=10°, Z=0.75; (b)** L^***=10,** $α$**=10°, Z=5; (c)** L^***=10,** $α$**=10°, Z=9.5; (d)** L^***=20,** $α$**=10°, Z=1.2; (e)** L^***=20,** $α$**=10°, Z=10; (f)** L^***=20,** $α$**=10°, Z=18.8; (g)** L^***=20,** $α$**=15°, Z=1.2; (h)** L^***=20,** $α$**=15°, Z=10; (i)** L^***=20,** $α$**=15°, Z=18.8; (j)** L^***=20,** $α$**=20°, Z=1.2; (k)** L^***=20,** $α$**=20°, Z=10; and (l)** L^***=20,** $α$**=20°, Z=18.8.**

4.2 Variation of the Velocity Vector

The velocity vector along the *Y-Z* plane is presented in Fig. 3a-f for L^*=10, Gr=1.08×10^5, S^*=0.20, C^*=0.10 at a respective inclination. All the variation of velocity vector for the *Y-Z* plane is plotted at *X*= 0.12; which is basically near the mid-section of the base. Also, primary focus has been paid to show velocity vectors near the exit (i.e., Z=9 to10) and the inlet (i.e., Z=0 to 1). Near the inlet, the reverse flow can be seen near the fin tip region, whereas, near the exit as mentioned in the above section the reverse velocity vectors are found near the base.

In Fig. 3a-f along the *Y-Z* plane when α is increased (from 10° to 20°) the velocity vectors are observed to have marginally changed in the magnitude, and in the clearance region, (i.e., beyond 1 in *Y*-axis) negligible or no change is reported. This may be due to the chimney effect, as 10° inclination is near to the horizontal position and the buoyancy force will act more towards the fin height at this position. And at 20° inclination (Fig. 3e-f), this effect increases towards the fin length. And directly a reduction in resistance is observed. Besides, the direction of the velocity vector is directly along with the fin height (i.e., *Y*-axis). Further, near *Y*= 0.6 to1 (i.e., near the top half of the fin or in other words from the middle to the fin tip) magnitude of the velocity vector can be seen to increase near the exit as the inclination increases.
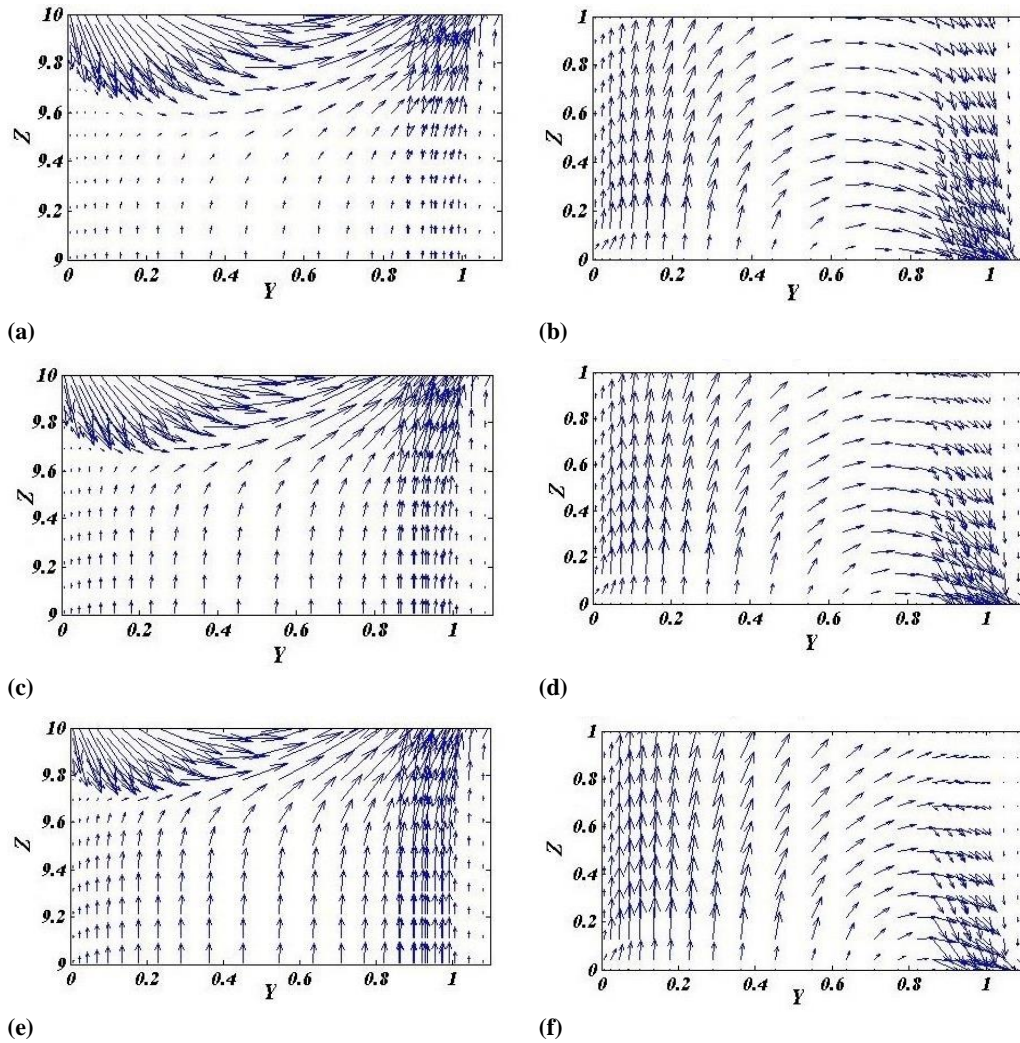
(a)

(b)

(c)

(d)

(e)

(f)

Fig. 3. Velocity vector plot near outlet and inlet at Y-Z plane, for L*=10, Gr=1.08×105, S*=0.2, C*=0.10, X=0.12 at (a) α=10° Z=9 to10, (b) α=10° Z=0 to 1, (c) α=15° Z=9 to 10, (d) α=15° Z=0 to 1, (e) α=20° Z=9 to 10, and (f) α=20° Z=0 to 1.

4.3 Variation of Bulk Temperature

The distribution of the temperature profile of fluid for Gr=1.08×10⁵, S^*=0.50, C^*=0.10 is plotted in Fig. 4a-h. At L^*=10, near the inlet (i.e., Z= 0.75) and outlet (i.e., Z= 9.5) and the variation in the profile is depicted in Fig.4a-b. Near the inlet, the temperature of the fluid in the mid-section of the fin base arrangement is lower than that of the exit section, due to the transfer of heat to the fluid. Form Fig. 4c, e, and g, near the inlet at L^*=20 the distribution with an increase in α, the profile volume can be seen to increase which directly signifies more heat distribution or transfer. This may be due to the improvement of the buoyancy force and the increase in the stack effect caused by increasing the inclination. Again, near the exit in Fig. 4d, f, and h (i.e., 10°, 15°, and 20°), the range of variation in the temperature profile can be seen to increase marginally causing an increase in heat transport at a higher inclination angle. Further, comparing Fig.4a with c, it can be concluded that, by increasing the

length of the channel by 100%, the range of volume of the temperature profile is reduced, which directly signifies lower heat transfer. It may be due to more resistance in fluid flow at higher length and less at lower length with enhancement in the chimney effect for respective inclination. This phenomenon of temperature variation at shorter length is also reported by Dialameh *et al*. (2008), but not for slight inclination.

4.4 Variation of fin temperature

The distribution of dimensionless fin temperature is illustrated and analyzed in Fig.5, 6, and 7. In Fig. 5a-c the effect of an increase in α (10°, 15°, and 20°) can be seen. The tip of the profile gets lower as α is increased or in other words, the profile expands on the *Y-Z* plane. This phenomenon can be explained as more heat removal takes place at a higher inclination causing a decrease in the dimensionless fin temperature. In Fig.6a-c, at an increased value of Grashof number (Gr) the change in the fin
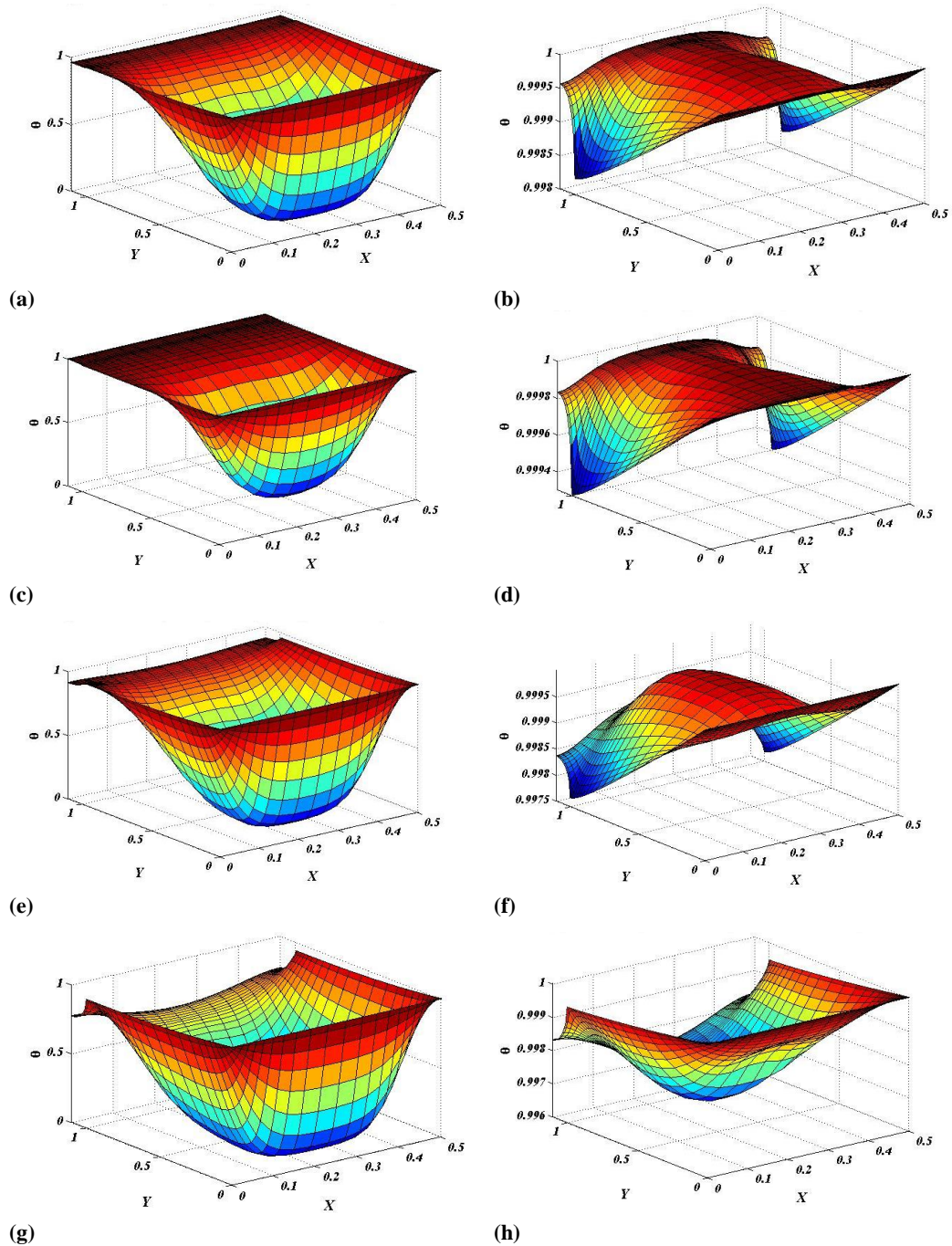
(a)

(b)

(c)

(d)

(e)

(f)

(g)

(h)

Fig. 4. Temperature profile for S*=0.5, C*=0.1, Gr=1.08×105 at (a) L*=10, α=10°, Z=0.75; (b) L*=10, α=10°, Z=9.5; (c) L*=20, α=10°, Z=1.2; (d) L*=20, α=10°, Z=18.8; (e) L*=20, α=15°, Z=1.2; (f) L*=20, α=15°, Z=18.8 (g) L*=20, α=20°, Z=1.2 and (h) L*=20, α=20°, Z=18.8.

temperature profile is significantly plotted. Here, it is exigent to express the Grashof number (Gr) only depends on the height of the fin as the temperature difference (80 °C) is kept constant for the present investigation. It is interesting to note that along the *Y*-axis the fin temperature is found to be higher for α=10°. This may be due to the existence of reverse flow, as the flow is not able to overcome the resistance and moves backward which doesn't allow fresh flow from the clearance region to enter and carry the heat. Further, it is clearly shown in the

subsequent plots for the non-dimensional fin tip to shroud increased clearance (C^*) (i.e., Fig.7a-c).

The area of the duct increases with the increase of the clearance (C^*). Therefore, comparing the results it can be seen that the area of the fin temperature profile increases with the increase in C^* which suggests a marginal increase in heat transfer at L^*= 20. Similar trends are also obtained by Roy *et al.* (2019) but at a different higher angle of inclination. This marginal variation also signifies the role of clearance, which provides the region for the fresh air or the working
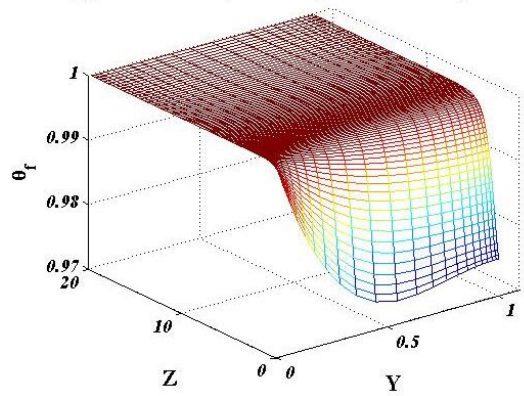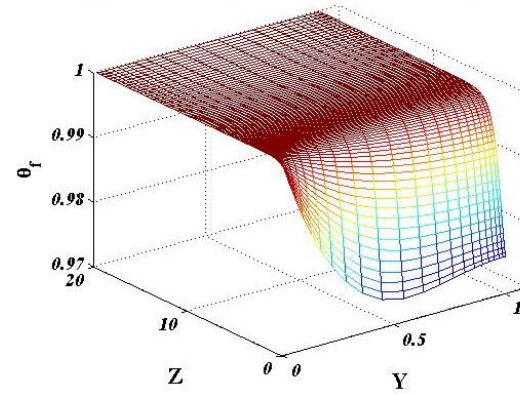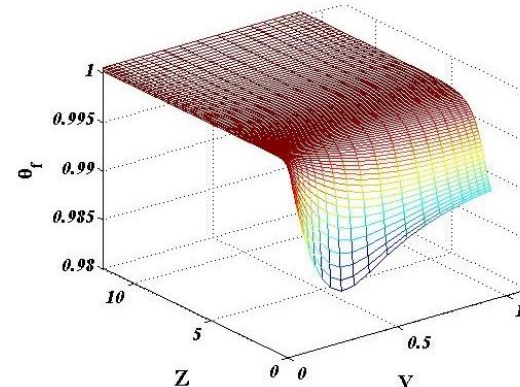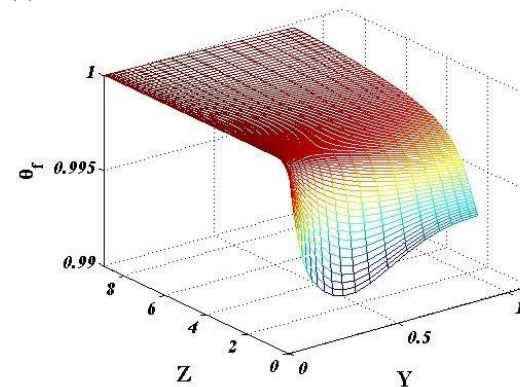
(a)
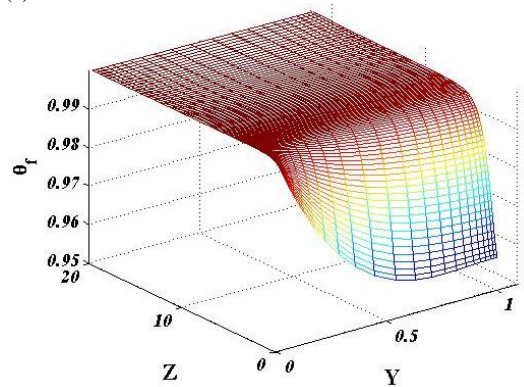
(b)
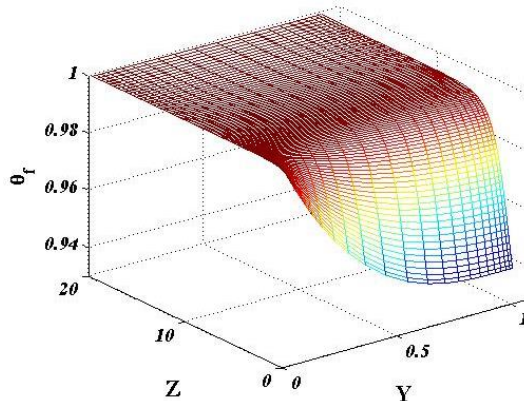
(c)

Fig. 5. Distribution of dimensionless fin temperature for various inclination angle at L^*=20, C^*=0.10, Gr=1.08×10⁵, S^*=0.3, (a) α=10°, (b) α=15°, and (c) α=20°.

(a)

(b)

(c)

Fig. 6. Distribution of dimensionless fin temperature for various Gr, at L^*=20 S^*=0.3, C^*=0.10, α=10°, (a) Gr=1.08×10⁵, (b) Gr=4.42×10⁵, (c) Gr=11.5×10⁵.

medium to remove heat. Also, the heat transfer rate it is obtained to be increasing with the increase in fin spacing. As it allows the air to circulate and carryout the heat.

4.5 Convective coefficient

The variation of the convective coefficient of heat transfer (*h*) (W/m² K) is presented in Fig.6. The variation at each inclination angle (α) for different clearance (*C**) at L^*=10 and 20, Gr=1.08×10⁵, S^*=0.2 and 0.5 is shown in Fig.8a and b, respectively. At a lower value of S^* the profile is quite expected, as the

L^* is increased the value of *h* reduces. Again, the value of *h* rises as the value of C^* increases from 0.1 to 0.3 (Fig.8a). Whereas at higher S^* (keeping other conditions same) the variation at α=10° and 15° is very different from α=20°. For L^*=10 and α=20°, a maximum of 18.5% increase in the value of h is obtained when C^* is increased from 0.1 to 0.3, but it reduces by 8.3% at α=10°. Increasing the inclination angle from 10° to 20°, the convective coefficient increases up to a maximum of 161 % for S^*=0.5, L^*= 10, C^*=0.3, and Gr=1.08×10⁵ (Fig.8b).
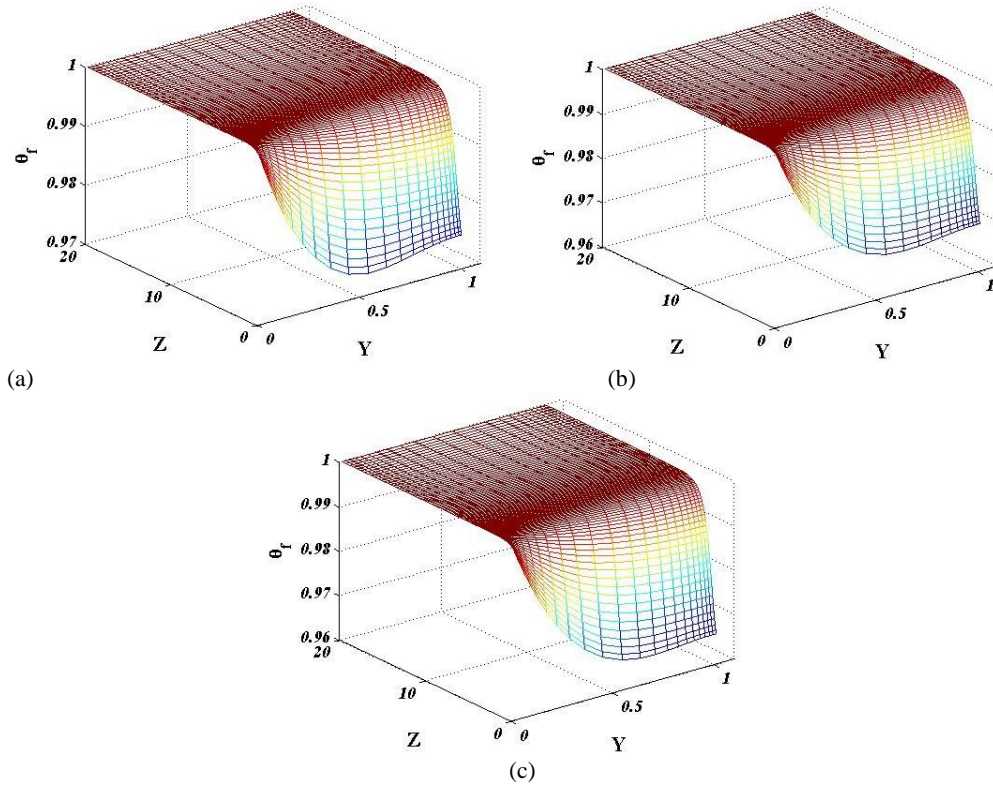
(a)

(b)

(c)

Fig. 7. Distribution of dimensionless fin temperature for various clearance, at L^*=20 S^*=0.3, α=10°, Gr=1.08×10^5 (a) C^*=0.10, (b) C^*=0.20, and (c) C^*=0.30.
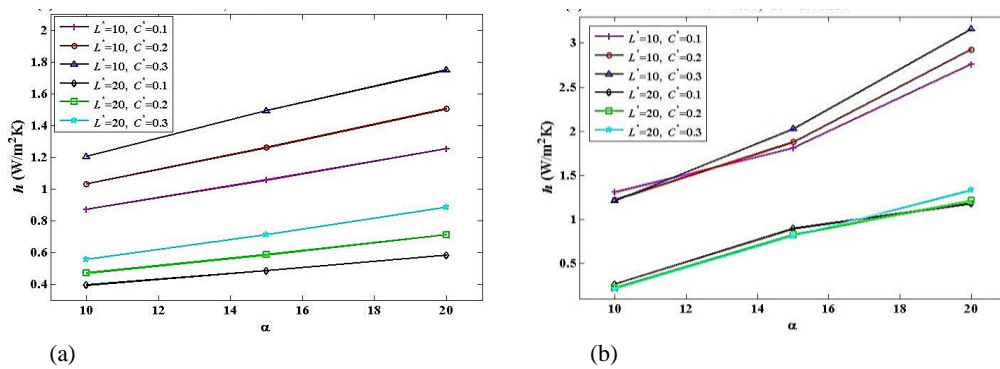

(a)

(b)

Fig. 8. Variation of convective heat transfer coefficient for different inclination angle, at L^*= 10 and 20, Gr=1.08×10^5, (a) S^*=0.2 and (b) S^*=0.5.
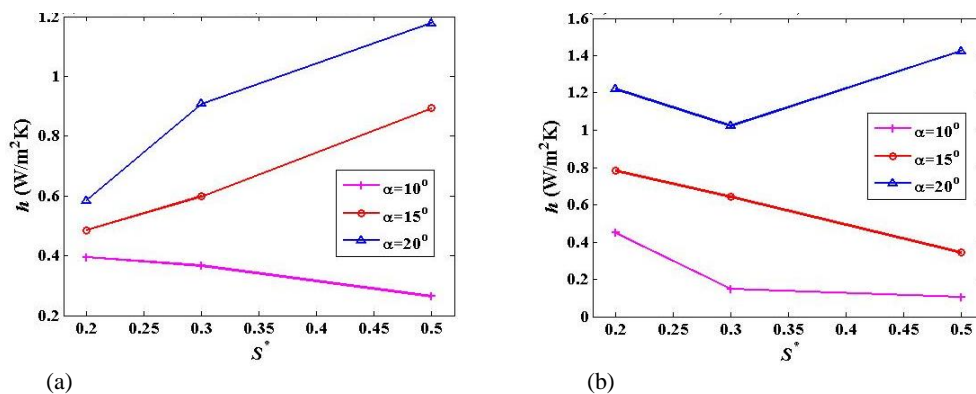

(a)

(b)

Fig. 9. Variation of convective heat transfer coefficient for different Spacing, at L^*= 20, C^*=0.1, (a) Gr=1.08×10^5 and (b) Gr=4.42×10^5.

Now, attention is paid to the variation of the convective coefficient with non-dimensional fin length (L^*) and it shows that the higher values of L^* will always possess a lesser heat transport coefficient than that of lower L^*. These solutions are in acceptable agreement with Mittelman *et al.* (2007), Dialameh *et al.* (2008), and Roy *et al.* (2019). The buoyancy force causes the natural convection thus the variation at each Grashof number is highly significant. From Fig.9a, it can be seen clearly that as the heat transfer coefficient value increases for α=15° and 20° but not for the lower value of the inclination. At α= 15° and 20°, the percentage enhancement of the heat transfer is of 84.1 and 101.6 respectively, while at α=10°, the same is reduced by 33.3%; while increasing the non-dimensional fin spacing from 0.2 to 0.5. Also, Fig.9b presents the variation of the heat transfer coefficient for L^*= 20, Gr=4.42×10^5 for each inclination. It shows that at lower values of non-dimensional fin spacing S^* as the value of α increases the h (W/m^{2}K) value increases directly. This trend changes completely as the value of S^* increases and at S^*= 0.5 with the increase in clearance from 0.1 to 0.3, the h value reduces.
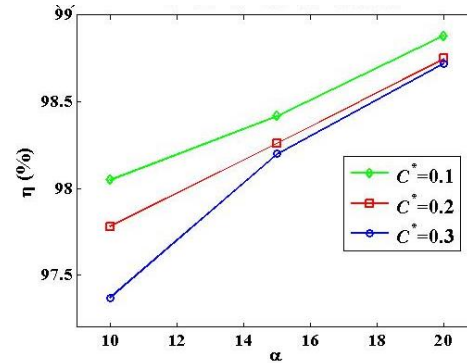
4.6 Variation of fin efficiency

Figure 10 illustrates the variation of fin efficiency (η) with spacing, and inclination angle. Fin efficiency is a significant indicator, which determines the deviation of actual to isothermal fin heat transfer, to practically increase or reduce the fin surface area while application. In Fig.10a at L^*=20, α=10°, Gr=1.08×10^5, for each C^* and S^* the trend is found to be initially reducing (i.e., for S^*=0.2 to 0.3) and then increasing (i.e., for S^*= 0.3 to 0.5). The initial decrease indicates that the increase in clearance is not that effective within the considered clearance at lower fin spacing, which is rare in literature. A decrease in efficiency with an increase in mass flow rate for a vertical channel may be observed in Das and Giri (2014), as such the present case may be well compared since with the increased clearance inlet mass flow rate is increased. However, at higher fin spacing a general trend is observed. Also, the variation of fin efficiency for different inclination angle (i.e., α=10°, 15°, and 20°) at S^*=0.2, L^*= 20, Gr=1.08×10^5 is plotted in Fig.10b. From the results, it is observed that efficiency always increases with the increase in α.

A maximum of 1.35% is obtained to be increased at lower S^* (i.e., from α=10° to 20°). Therefore, the reducing trend of efficiency, for the case α=10° to 20° (when C^* is increased from 0.1 to 0.3), may be due to the relatively lesser cooling capacity of decreased mass flow rate. Moreover, it is also associated with the chimney effect created due to a marginal reduction in the inclination (i.e., towards a horizontal position) of the base-fin system. Scarcely any existing investigation remains which indicate such a trend for a slight inclination of fin base system. In general, fin efficiency increases with a marginal increase in inclination which is highly appreciable.
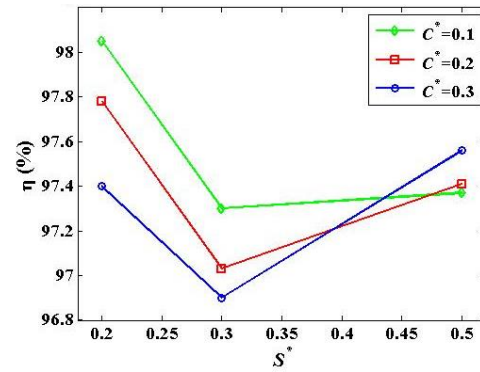
(a)

(b)

Fig. 10. Variation of fin efficiency for different (a) spacing at L^*= 20, α=10°, Gr=1.08×10^5, and (b) inclination angle at S^*=0.2, L^*= 20, Gr=1.08×10^5.

5. CONCLUSION

Computational investigations are performed for natural convective heat transfer in a slightly inclined channel (α=10°, 15°, and 20°). For L^*=10, the occurrence of reverse flow is inevitable; whereas at higher length only near the clearance region its presence is reported. Thus, its dependence on length and inclination is clearly illustrated. The following conclusions are made for the present investigation:

• From the *W*-velocity profile, near the entrance, flow reversal is reduced with the increase of inclination angle (α) but its presence in the clearance region is common to all the chosen cases.

• With the slight increase in the inclination angle, the volume of the temperature profile of the fluid is found to be increased gradually.

• The magnitude of the velocity vector is obtained to be reduced as the inclination angle increases near 0.6 to 1 on the *Y*-axis.

• Along the *Y*-axis the fin temperature is observed to increase at α=10°; which is particularly reported only for α=10°. This phenomenon may be due to the presence of reverse flow.

• Increase in the angle of inclination from 10° to 20°, the convective coefficient increases up to a maximum of 161 % for S^*=0.5, L^*= 10, C^*=0.3, and Gr=1.08×10^5.

- For all the considered inclination and Grashof number, and at lower fin spacing (i.e., S^*<0.3), fin efficiency is found to decrease with an increase in C^*. However, at higher spacing, efficiency increases with clearance.

- For lower inclination angle of α =10° and $S^* = 0.2$, the fin efficiency decreases as the Grashof number (Gr) increases from 1.08×10^5 to 11.5×10^5. This reduction is limited to 8.6%.

REFERENCES

Ahmed, H. E. (2016). Optimization of thermal design of ribbed flat-plate fin heat sink. *Applied Thermal Engineering* 102, 1422-1432.

Al-Sarkhi, A., E. Abu-Nada, B. A. Akash and J. O. Jaber (2003). Numerical investigation of shrouded fin array under combined free and forced convection. *International Communications in Heat Mass Transfer* 30, 435-444.

Alta, D., E. Bilgili, C. Ertekin and O. Yaldiz (2010). Experimental investigation of three different solar air heaters: Energy and exergy analyses. *Applied Energy* 87, 2953-2973.

Boutina, L. and R. Bessaïh (2011). Numerical simulation of mixed convection air-cooling of electronic components mounted in an inclined channel. *Applied Thermal Engineering* 31, 2052-2062.

Chen, H. T., H. C. Tseng, S. W. Jhu and J. R. Chang (2017). Numerical and experimental study of mixed convection heat transfer and fluid flow characteristics of plate-fin heat sinks. *International Journal Heat Mass Transfer* 111, 1050-1062.

Das, B. and A. Giri (2014). Non-Boussineśq laminar mixed convection in a non-isothermal fin array. *Applied Thermal Engineering* 63, 447–458.

Davoodi, H. and M. Yaghoubi (2018). Experimental and numerical study of natural convection heat transfer from arrays of zigzag fins. *Heat and Mass Transfer* 55 (7), 1913-1926.

Dialameh, L., M. Yaghoubi and O. Abouali (2008). Natural convection from an array of horizontal rectangular thick fins with short length. *Applied Thermal Engineering* 28, 2371-2379.

Dindarloo, M. R. and S. Payan (2019). Effect of fin thickness, grooves depth, and fin attachment angle to the hot wall on maximum heat transfer reduction in a square enclosure. *International Journal of Thermal Science* 136, 473-490.

Feng, S., M. Shi, H. Yan, S. Sun, F. Li and T. J. Lu (2018). Natural convection in a cross-fin heat sink. *Applied Thermal Engineering* 132, 30-37.

Fisher, T. S. and K. E. Torrance (1999). Experiments on chimney-enhanced free convection, Trans. ASME. *Journal of Heat Transfer* 121, 603-609.

Ghandouri, I. El., A. El Maakoul, S. Saadeddine and

M. Meziane (2020). Design and Numerical Investigations of Natural Convection Heat Transfer of a New Rippling Fin Shape. *Applied Thermal Engineering* 178, 115670

Giri, A. and B. Das (2012). A numerical study of entry region laminar mixed convection over shrouded vertical fin arrays. *International Journal of Thermal Science* 60, 212-224.

Harahap, F. and H. N. McManus (1967). Natural convection heat transfer from horizontal rectangular fin arrays. *Journal of Heat Transfer* 89, 32-38.

Hasan, Md. N., C. Chowdhury, K. A. Jewel and S. Saha (2017). A Computational Study on Mixed Convection Heat Transfer in an Inclined Rectangular Channel under Imposed Local Flow Modulation. *Journal Chemical Engineering IEB* 30 (1), 43-50.

Homod, R. Z., F. A. Aboodb, S. M. Shramab and A. K. Alsharac (2019). Empirical correlations for mixed convection heat transfer through a fin array based on various orientations. *International Journal of Thermal Science* 137, 627-639.

Huang, X., C. Shi, J. Zhou, X. Lu and G. Xu (2019). Performance analysis and design optimization of heat pipe sink with a variable height fin array under natural convection. *Applied Thermal Engineering* 159 113939.

Jeon, D. and C. Byon (2017). Thermal performance of plate-fin heat sinks with dual-height fins subject to natural convection. *International Journal of Heat and Mass Transfer* 113, 1086-1092.

Karki, K. C. and S. V. Patankar (1987). Cooling of a vertical shrouded fin array by natural convection: a numerical study. *Journal of Heat Transfer* 109, 671-676.

Karlapalem, V., S. Rath and S. K. Dash (2019). Orientation effects on laminar natural convection heat transfer from branching-fins. *International Journal of Thermal Science* 142, 89-105.

Leung, C. D., S. D. Probert, and M. J. Shilston (1985). Heat exchangers: Optimal separation for vertical rectangular fins protruding from a vertical rectangular base. *Applied Energy* 19, 77-85.

Mehrtash, M. and I. Tari (2013). A correlation for natural convection heat transfer from inclined plate-finned heat sinks. *Applied Thermal Engineering* 51, 1067-1075.

Meng, X., J. Zhu, X. Wei and Y. Yan (2018). Natural convection heat transfer of a straight-fin heat sink. *International Journal of Heat and Mass Transfer* 123, 561-568.

Micheli, L., K. S. Reddy and T. K. Mallick (2016) Experimental comparison of micro-scaled plate-fins and pin-fins under natural convection.

International Communications in Heat and Mass Transfer 75, 59-66.

Mittelman, G., A. Dayan, K. D. Turjeman and A. Ullmann (2007). Laminar free convection underneath a downward facing inclined hot fin array. *International Journal of Heat and Mass Transfer* 50 (13), 2582-2589.

Mousavi, H., A. A. R. Darzi, M. Farhadi and M. Omidi (2018). A novel heat sink design with interrupted, staggered and capped fins. *International Journal of Thermal Science* 127, 312-320.

Patankar, S. V. (1980). Numerical Heat Transfer and Fluid Flow, Hemisphere, Washington DC.

Pathak, K. K., A. Giri and P. Lingfa (2018). A numerical study of convective heat transfer from a shrouded vertical variable height non-isothermal fin array. *Applied Thermal Engineering* 130, 1310-1318.

Roy, K. and B. Das (2019). Effect of Property Variation on the Fluid Flow and Thermal Behavior in a Vertical Channel. *Journal of Applied Fluid Mechanics* 12(4), 1177-1188.

Roy, K. and B. Das (2020). Convective heat transfer from an inclined isothermal fin array: A computational study. *Thermal Science and Engineering Progress* 17 100487.

Roy, K. and B. Das (2021). Influence of property variation on natural convection in a vertical finned channel: An extended study. *Journal of Thermal Science and Engineering Applications* 13(3), 031019.

Roy, K., A. Giri and B. Das (2019). A computational study on natural convection heat transfer from an inclined plate finned channel. *Applied Thermal Engineering* 159, 113941.

Shen, Q., D. Sun, Y. Xu, T. Jin and X. Zhao (2014). Orientation effects on natural convection heat dissipation of rectangular fin heat sinks mounted on LEDs. *International Journal of Heat and Mass Transfer* 75, 462-469.

Shi, X., S. Li, Y. Mu and B. Yin (2019). Geometry parameters optimization for a microchannel heat sink with secondary flow channel. *International Communications in Heat and Mass Transfer* 104, 89-100.

Starner, K. E. and H. N. McManus (1963). An experimental investigation of free-convection heat transfer from rectangular-fin arrays. *Journal of Heat Transfer* 85, 273-278.

Tari, I. and M. Mehrtash (2013). Natural convection heat transfer from inclined plate-fin heat sinks. *International Journal of Heat and Mass Transfer* 56, 574-593.

Tari, I. and M. Mehrtash (2013a). Natural convection heat transfer from horizontal and slightly inclined plate-fin heat sinks. *Applied Thermal Engineering* 61, 728-736.

Welling, J. R. and C. V. Wooldridge (1965). Free convection heat transfer coefficients from rectangular vertical fins. *Journal of Heat Transfer* 87, 439-444.

Yang, M. H. and R. H. Yeh (2019). Optimization of fin arrays in an inclined channel for mixed convection. *Applied Thermal Engineering* 148, 963-976.

Zhang, X., Y. Wang, Z. Yu and D. Zhao (2015). Numerical analysis of thermal-hydraulic characteristics on serrated fins with different attack angles and wavelength to fin length ratio. *Applied Thermal Engineering* 91 126-137.